Fast voice-coil scanning optical-resolution photoacoustic microscopy

Lidai Wang, Konstantin Maslov, Junjie Yao, Bin Rao, and Lihong V. Wang*

Optical Imaging Laboratory, Department of Biomedical Engineering, Washington University in St. Louis, Campus Box 1097, One Brookings Drive, St. Louis, Missouri 63130-4899, USA

**Corresponding author: lhwang@biomed.wustl.edu*

Received September 22, 2010; revised November 24, 2010; accepted November 27, 2010; posted December 13, 2010 (Doc. ID 135532); published January 6, 2011

We developed a photoacoustic imaging system that has real-time imaging capability with optical resolution. The imaging system is capable of scanning at 20 Hz over a 9 mm range and up to 40 Hz over a 1 mm scanning range. A focused laser beam provides a lateral resolution of 3.4 μm as measured in an optically nonscattering medium. Flows of micrometer-sized carbon particles or whole blood in a silicone tube and individual red blood cells (RBCs) in mouse ear capillaries were also imaged in real time, demonstrating the capability to image highly dynamic processes *in vivo* at a micrometer-scale resolution. © 2011 Optical Society of America

OCIS codes: 170.3880, 170.5120, 180.5810.

Photoacoustic tomography (PAT), detecting ultrasound signals generated from photon absorption, provides optical absorption contrast *in vivo* for structural, functional, and molecular imaging [1–4]. PAT has two major modes: computed tomography (PACT) and focused-scanning tomography (PAM). In PAM, a single focused ultrasound transducer is mechanically scanned across a two-dimensional plane to acquire a three-dimensional image. At each scanned position, the acoustic time-of-flight provides depth information, and the acoustic focusing (AR-PAM) [4] or optical focusing (OR-PAM) [5] yields lateral resolution. Compared with PACT, PAM has a simpler implementation. Moreover, the spatial resolution of PAM can be scaled to image objects from subcellular organelles to organs [6]. However, most PAM systems utilize a precise ball-screw scanning mechanism, making it inherently difficult to achieve high scanning speed. This limitation calls for new technology to image dynamic processes *in vivo* with high spatial resolution. Fast scanning speed can sufficiently reduce the time to acquire a image so that dynamic processes can be imaged and motion artifacts can be mitigated. A high-speed voice-coil stage has been used to improve the scanning speed in an AR-PAM system, but only slow photoacoustic imaging was demonstrated [7]. Another PAM modality employed optical scanning with weak acoustic focusing to improve scanning speed [8]; however, the weak acoustic focusing limited signal-to-noise ratio (SNR).

We present a PAM system that can provide real-time cross-sectional (B-scan) imaging with optical lateral resolution. The system utilizes a voice-coil linear translation stage to achieve high-speed scanning. Tight optical focusing provides a high lateral resolution of 3.4 μm in optically nonscattering medium.

As shown in Fig. 1, a pulsed laser delivers light to the photoacoustic scanning probe through a single mode optical fiber. The laser beam is focused by a set of optical lenses and then reflected on an aluminum-coated prism. The delivered laser pulse energy may vary from several tens of nanojoules to over 100 nJ. An ultrasound transducer (V2022 BC, Olympus NDT) is employed to detect photoacoustic signals. The ultrasound transducer focuses on the same spot as the optical beam through two prisms and an acoustic concave lens (6 mm aperture, 0.5 NA in water). The optical and acoustic components are attached to a base plate to form a scanning probe, which weighs less than 40 g.

The scanning probe is mounted on a voice-coil linear translation stage (VCS-1010, Equipment Solutions, Sunnyvale, CA, USA), to create a fast-scanning axis (x axis). Photoacoustic signals are amplified by two amplifiers (ZFL-500LN+, Mini-circuits, NY, USA) and then acquired by a high-speed digitizer (DAQ) (ATS9350, Alazar Tech Inc., Pointe-Claire, QC, Canada), using a sampling rate of 500 MHz. The imaging system is capable of scanning at 20 Hz over a 9 mm range and up to 40 Hz over a 1 mm range. The B-scan frame rate of the imaging system is currently limited by the laser repetition rate of 4 kHz. In this Letter, we demonstrate fast scanning ability over small scanning ranges. However, the scanning range can be readily increased by using a faster pulsed laser without sacrificing the scanning speed. The fast B-scan speed shortens the time to acquire a volumetric image, and the imaging system can work in a repetitive B-scan mode to image highly dynamic processes in real time.

As shown in Fig. 2(a), the lateral resolution of the PAM system was quantified by imaging a sharp edge in water. The FWHM of the line spread function was 3.4 μm. The axial resolution was estimated to be 15 μm by the system

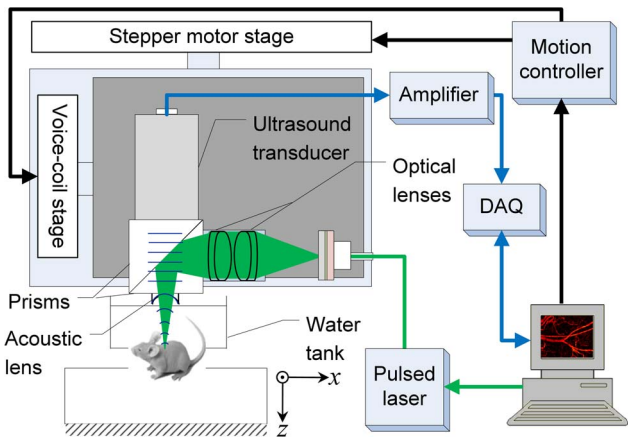

Fig. 1. (Color online) Schematic of voice-coil-driven fast-scanning OR-PAM.

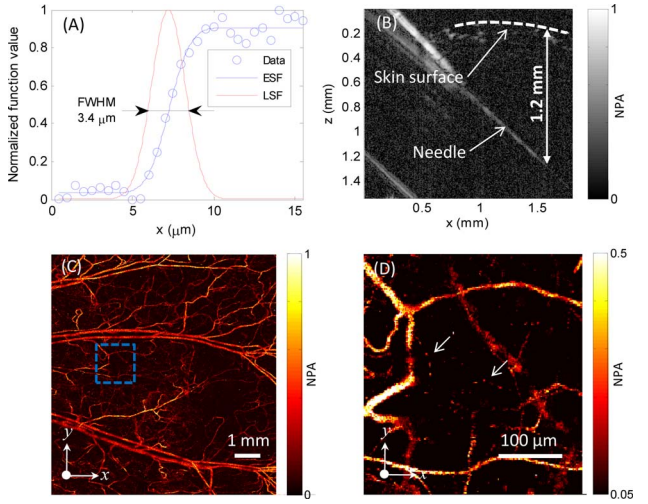

Fig. 2. (Color online) (A) Lateral resolution test on a sharp edge. ESF, edge spread function; LSF, line spread function. (B) Test of penetration depth by imaging a needle obliquely inserted into biological tissue. (C) *In vivo* maximum amplitude projection (MAP) image of mouse ear vasculature. (D) Close-up of the region enclosed by the dashed box in (C); arrows denote capillaries. NPA, normalized photoacoustic amplitude.

bandwidth of 100 MHz and the speed of sound in biological tissue (~1.5 μm/ns). The penetration depth of the PAM was measured by imaging a needle inserted obliquely into the leg of a living mouse. As shown in Fig. 2(b), the needle is visible at a depth of 1.2–1.4 mm into the tissue. Figure 2(c) shows an image of the microvasculature in a nude mouse ear acquired *in vivo* at an optical wavelength of 570 nm. Figure 2(d) is a close-up image of the region indicated by the dashed box in Fig. 2(c). Capillaries, the smallest blood vessel, are clearly resolved.

The SNR of the imaging system was measured by imaging a slice cut from a graphite rod (99.995%, Sigma-Aldrich Co., St. Louis, Missouri, USA). The laser energy was 40 nJ per pulse, and the average SNR was 45 dB.

Flows of carbon particles with a mean diameter of 6 μm were imaged in real time in repetitive B-scan mode. As shown in Fig. 3(a), a syringe pump was used to control the flow speed. The PAM scanned in parallel with the tube at 20 Hz. Figure 3(b) shows a representative B-scan image. The high-resolution real-time B-scan images provided the flow speed distribution along the depth direction of the tube. Figure 3(c) shows the distribution along the x axis of the photoacoustic signal at one depth as a function of time. The slope of each carbon particle trajectory is proportional to the flow speed at this depth. In the time domain, the flow speed v at the depth z can be written as $v(z) = k\frac{\Delta x}{\Delta t + \frac{\Delta x}{v_s}} = k\frac{1}{1+\frac{\Delta x/\Delta t}{v_s}}\frac{\Delta x}{\Delta t}$, where k is a constant coefficient and v_s is the scanning speed. When the scanning speed is much higher than the flow speed, which is the case here, the term $\frac{\Delta x/\Delta t}{v_s}$ can be disregarded. The flow speed can be approximated with $v(z) = k\frac{\Delta x}{\Delta t}$. The flow speed can be more robustly calculated in the frequency domain. The two-dimensional Fourier transform of the data in Fig. 3(c) is shown in Fig. 3(d). F_t and F_x are the temporal and spatial frequencies associated with t and x, respectively. From the Fourier

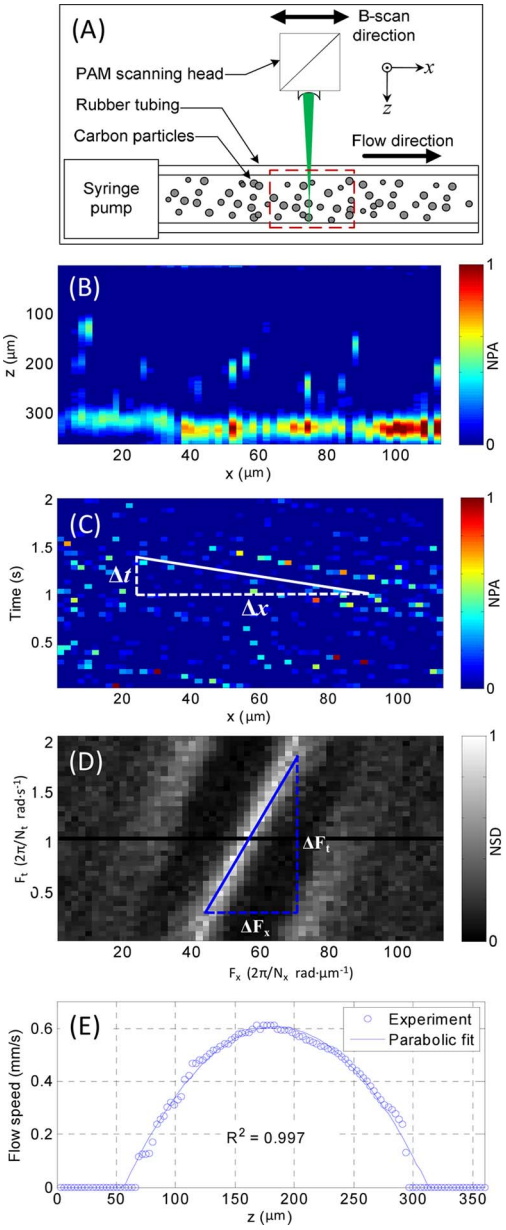

Fig. 3. (Color online) (A) Schematic of the experiment setup for carbon particle flow measurement. (B) Representative B-scan flow image across the dashed-box area in (A). (C) Distribution of imaged carbon particles along the x axis at one z axis position versus time. (D) Frequency spectrum of data in (C) obtained with two-dimensional Fourier transformation. (E) Imaged parabolic flow speed along the z axis. NPA, normalized photoacoustic amplitude; NSD, normalized spectrum density.

transformation, we have $\Delta F_t = \frac{2\pi}{N_t}\frac{1}{\Delta t}$, $\Delta F_x = \frac{2\pi}{N_x}\frac{1}{\Delta x}$, where N_t and N_x are the sample lengths in the t and x axes, respectively. Hence, the flow speed v can be rewritten as $v(z) = k\frac{\Delta x}{\Delta t} = k\frac{N_t}{N_x}\frac{\Delta F_t}{\Delta F_x}$. Using the syringe pump, the coefficient k was calibrated to be 2.2. As shown in Fig. 3(e), a parabolic flow distribution along the depth direction was computed based on the real-time photoacoustic images.

Flows of whole bovine blood in a rubber tube were imaged at a 20 Hz B-scan rate. Variations in concentrations of RBCs were resolved. Figure 4(a) shows a representative B-scan image. By changing the speed of the syringe

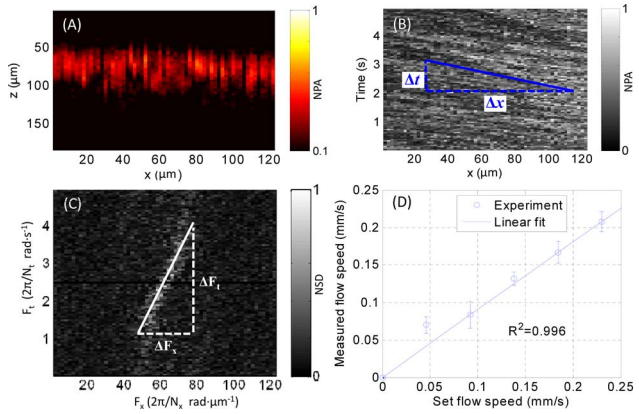

Fig. 4. (Color online) (A) B-scan image of whole blood flowing in a tube. (B) MAP along the z axis of the B-scan image versus time. (C) Two-dimensional frequency spectrum of the data in (B). (D) Measured flow speed versus the preset values. NPA, normalized photoacoustic amplitude; NSD, normalized spectrum density.

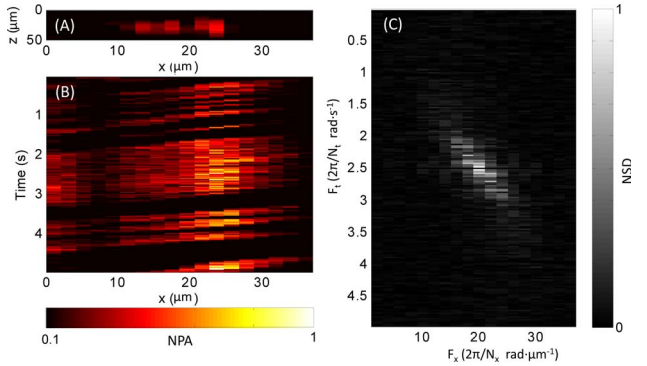

Fig. 5. (Color online) (A) *In vivo* B-scan of single RBCs flowing in a mouse ear capillary. (B) MAP along the z axis of the B-scan image versus time (Media 1). (C) Two-dimensional frequency spectrum of the data in (B). NPA, normalized photoacoustic amplitude; NSD: normalized spectrum density.

pump, the flow speed within the penetration depth was varied from 0.04 to 0.25 mm/s. The same calibration k used for the carbon particle flow was employed to compute the blood flow speed. The measured flow speeds, as shown in Fig. 4(d), agree with the preset flow speed.

In a nude mouse ear, individual RBCs traveling in a capillary were imaged *in vivo* at a B-scan rate of 40 Hz. Figure 5 shows individual RBCs flowing in the capillary, and a real-time video for individual RBCs flowing (Media 1) is attached. The flow speed was computed in the frequency domain, as shown in Fig. 5(c), using the coefficient k calibrated in the carbon particle flow experiment. Over 5 s, the average flow speed in the capillary was 0.13 mm/s, with a standard deviation of 0.03 mm/s.

All experimental animal procedures were carried out in conformance with the laboratory animal protocol approved by the Animal Studies Committee of Washington University in St. Louis.

To our knowledge, this is the first time PAM has demonstrated fast scanning capability at a frame rate of up to 40 Hz with optical resolution. Fast scanning OR-PAM can improve the imaging efficiency by tens of times, image highly dynamic processes in real time, and potentially reduce motion artifacts. This provides potentially broad applications. One example is functional imaging of RBC flows in a capillary *in vivo*. Although other imaging technologies, such as confocal microscopy, two-photon microscopy, and optical coherent tomography also can image RBC flows in a capillary *in vivo*, none of them can provide optical absorption contrast. Moreover, OR-PAM can measure oxygen saturation (SO_2), which is an important parameter for functional imaging.

We acknowledge the help of Li Li in the system design. This work was sponsored in part by National Institutes of Health (NIH) grants R01 EB000712, R01 EB008085, R01 CA134539, U54 CA136398, R01 EB010049, and 5P60 DK02057933. L. V. Wang has a financial interest in Microphotoacoustics, Inc. and Endra, Inc.; however, neither provided support for this work.

References

1. X. Wang, Y. Pang, G. Ku, X. Xie, G. Stoica, and L. V. Wang, Nat. Biotechnol. **21**, 803 (2003).
2. J. A. Copland, M. Eghtedari, V. L. Popov, N. Kotov, N. Mamedova, M. Motamedi, and A. A. Oraevsky, Mol. Imaging Biol. **6**, 341 (2004).
3. R. I. Siphanto, K. K. Thumma, R. G. M. Kolkman, T. G. van Leeuwen, F. F. M. de Mul, J. W. van Neck, L. N. A. van Adrichem, and W. Steenbergen, Opt. Express **13**, 89 (2005).
4. H. F. Zhang, K. Maslov, G. Stoica, and L. V. Wang, Nat. Biotechnol. **24**, 848 (2006).
5. K. Maslov, H. F. Zhang, S. Hu, and L. V. Wang, Opt. Lett. **33**, 929 (2008).
6. L. V. Wang, Nat. Photon. **3**, 503 (2009).
7. T. Harrison, J. C. Ranasinghesagara, H. Lu, K. Mathewson, A. Walsh, and R. J. Zemp, Opt. Express **17**, 22041 (2009).
8. Z. Xie, S. Jiao, H. F. Zhang, and C. A. Puliafito, Opt. Lett. **34**, 1771 (2009).